05,13

Effect of the thickness and tungsten alloying of Cr—Mn antiferromagnetic layers on the microstructure and hysteresis properties of Cr-Mn/FM type films ($FM = \text{Fe}_{20}\text{Ni}_{80}$, $\text{Fe}_{10}\text{Co}_{90}$, $\text{Fe}_{60}\text{Co}_{20}\text{B}_{20}$)

© A.A. Feshchenko¹, M.E. Moskalev¹, A.A. Ushkov¹, S.V. Semenova¹, V.N. Lepalovskij¹ E.A. Kravtsov^{1,2} V.O. Vas'kovskiy^{1,2}

¹ Ural Federal University after the first President of Russia B.N. Yeltsin, Yekaterinburg, Russia

 $^{2}\,\mathrm{M.N.}$ Mikheev Institute of Metal Physics, Ural Branch, Russian Academy of Sciences,

Yekaterinburg, Russia

E-mail: a.a.feshchenko@urfu.ru

Received March 6, 2025 Revised March 6, 2025 Accepted May 5, 2025

The patterns of changes in the coercive force and the exchange bias field of a number of iron-containing ferromagnetic layers FM = Fe, $\text{Fe}_{20}\text{Ni}_{80}$, $\text{Fe}_{10}\text{Co}_{90}$, $\text{Fe}_{60}\text{Co}_{20}\text{B}_{20}$ in $\text{Cr}_{70}\text{Mn}_{30}/\text{FM}$ films have been determined with varying thickness of the $\text{Cr}_{70}\text{Mn}_{30}$ antiferromagnetic layer and its doping W. The interpretation of the results obtained is based on the low stability of the magnetic state of the crystallites composing the antiferromagnetic layer. It is shown that it can be increased due to an increase in the volume of crystallites with an increase in the thickness of the antiferromagnetic layer. In this case, the final result largely depends on the specifics of the interlayer exchange interaction between the antiferromagnetic layer and ferromagnetic layers of various compositions. It was also found that the introduction of W weakens the magnetic anisotropy of the Cr_{-}Mn antiferromagnetic layer, but has a positive effect on the reproducibility of the hysteresis properties of film composites.

Keywords: antiferromagnet, ferromagnet, layering, composition, texture, thickness, temperature, coercive force, exchange bias, alloying.

DOI: 10.61011/PSS.2025.06.61708.19HH-25

1. Introduction

Ferromagnetic/antiferromagnetic type film structures are included in the range of modern functional media that are used in sensorics and spintronics areas [1,2]. such structures, the antiferromagnetic material serves as a source of exchange pinning of the magnetic moment in the adjacent ferromagnetic layer, i.e. stabilization of its homogeneously magnetized state. It is displayed in the form of a hysteresis loop shift along the magnetic field axis by $H_{\rm ex}$ called the exchange bias field [3,4]. However, it is important that this effect persists in a wide temperature range, including room temperature, and the substance has high specific electrical resistance, when it comes to magnetoresistive transducers, and good corrosion resistance [5,6]. Mn alloys with a number of platinum metals, in particular the Ir-Mn system, are a perfect example of antiferromagnetic materials [7,8]. However, a cost-demanding nature of these alloys incentivizes the search for alternative film structures based on antiferromagnetic Such antiferromaterials with high Neel temperature. magnetic materials, in particular, include Cr-Mn alloys whose Neel temperature may be higher than 600 K [9,10]. Meanwhile, previous studies of multilayer films, including Cr-Mn layers, indicate low magnetic anisotropy of this material [11–15]. This imposes a severe restriction on using

this material in film media with exchange bias because it implies that the antiferromagnetic vector of the pinning layer has a considerable stability with respect to the tilting action from the exchange-coupled ferromagnetic layer. The antiferromagnetic layer in ion-beam deposited multilayer films generally has a polycrystalline microstructure whose magnetic state stability is individual to each crystallite and is defined by the magnitude of its magnetic anisotropy energy [16]:

$$\varepsilon_a = K_a \cdot V, \tag{1}$$

where K_a is the crystalline magnetic anisotropy constant, and V is the crystallite volume.

Thus, the stability of antiferromagnetic crystallites, i. e. ε_a , may be increased by means of increasing the volume of crystallites or changing the anisotropy constant, for example, by doping. The latter, according to the literature [17–19], is quite effective in doping a Pt binary alloy and also works well when using Cu, Pd, Rh and Ir as dopants [20]. The objective of this work was to study the influence of both factors on the structure and hysteresis properties of the Cr-Mn/FM type film systems, which are indicative of magnetic stability of an antiferromagnetic layer. To achieve the magnetic stability, the antiferromagnetic layer thickness, to which the crystallite volume is usually related, was varied and the Cr-Mn films were doped with tungsten. The latter is more cost-attractive compared with platinum metals

and at the same time, as reported in [21,22], can increase the crystalline anisotropy of 3d-metal alloys. In addition, a structural characteristic of the ferromagnetic (FM) layer was added to the range of variable factors. The following set of FM materials was used for this: Fe having a BCC lattice; Fe₂₀Ni₈₀ and Fe₁₀Co₉₀ alloys with a FCC lattice; amorphous Fe₆₀Co₂₀B₂₀ alloy.

2. Experiment procedure

The experiment was conducted on films with the following multilayer structure:

```
\begin{array}{l} {\rm glass/Ta(5)/Cr_{70}Mn_{30}(\it{L})/FM(10)/Ta(5),} \\ {\rm glass/Ta(5)/Cr_{70}Mn_{30}(\it{L})/Ta(5),} \\ {\rm glass/Ta(5)/(Cr_{70}Mn_{30})_{100-\it{x}}W_{\it{x}}(\it{L})/Fe_{20}Ni_{80}(10)/Ta(5),} \\ {\rm glass/Ta/(Cr_{70}Mn_{30})_{100-\it{x}}W_{\it{x}}(\it{L})/Ta(5).} \end{array}
```

The given structural formulas show layer thicknesses in nanometers in brackets, including the variable value of L of the structure. Samples were prepared by the magnetron sputtering method implemented using the AJA ATC Orion-8 system. Residual gas pressure in the system's vacuum chamber was not higher than $5 \cdot 10^{-7}$ mm Hg. Metal sputtering was carried out in Ar (99.999%) at $2 \cdot 10^{-3}$ mm Hg. Corning cover slips, $25 \times 25 \times 0.2$ mm³, or NaCl crystals with an area of $5 \times 5 \text{ mm}^2$ were used as substrates. A substrate holder was subjected to highfrequency electrical bias of 14 W with a 250 Oe permanent homogeneous magnetic field (process field) existing in its Multilayer components of film structures were essentially formed using alloy targets. $Cr_{70}Mn_{30}$ and $(Cr_{70}Mn_{30})_{100-x}W_x(L)$, that were deposited in a singlecomponent target co-sputtering mode, were an exception.

The Nanohunter X-ray fluorescence spectrometer was used to control the chemical composition of films. The Dektak 150 stylus profiler was used to measure the total thickness of multilayer films. Partial layer thicknesses were set by calculation with respect to deposition time and predefined deposition rates of various materials. Crystal structure of the tested films was qualified using the PANalytical Empyrean series 2 X-ray diffractometer in $Co K_a$ radiation, and the JEOL JAM-2100 transmission electron microscope with an accelerating voltage of 200 kV. Magnetic properties of the samples were measured using the EvicoMagnetics Kerr-magnetometer and LakeShore vibrating sample magnetometer.

Properties of Cr₇₀Mn₃₀/FM films with a variable antiferromagnetic layer thickness

It was found earlier in [12] that the exchange bias effect in films containing Cr—Mn layers was observed at Mn concentration ranging from 20 to 40 at.%. Taking this into account, the study was conducted using $Cr_{70}Mn_{30}$. Figure 1 shows dependences of the coercive force H_c and exchange bias field $H_{\rm ex}$ on the thickness of an antiferromagnetic layer

Properties of ferromagnetic alloys in bulk (a, M_s) and film (H_c^*) states. Exchange bias effect characteristics $(H_c, H_{\rm ex}, K_e, T_b)$ of the ${\rm Cr}_{70}{\rm Mn}_{30}/FM$ film structures

FM	Features			
	Fe	Fe ₂₀ Ni ₈₀	Fe ₁₀ Co ₉₀	Fe ₆₀ Co ₂₀ B ₂₀
Type of structure	bcc	fcc	fcc	amorphous
a, nm	0.286	0.355	0.356	_
Ms, Gs	1710	810	1500	1200
H_c^* , Oe (film)	15	1	12	3
H_c , Oe (composite)	55	25	170	40
H _{ex} , Oe	20	23	17	9
K_e , erg/cm ³	0.035	0.02	0.025	0.01
T_b, K	540	510	560	600

with the specified composition. They were determined from magnetooptical hysteresis loops having a near-rectangular form as a loop halfwidth and a field of loop center shift along the magnetic field axis, respectively. Samples with different FM layers may be conditionally divided by these characteristics into two groups. Films from the first group $(FM = Fe_{20}Ni_{80}, Fe)$ feature an almost threshold nature of $H_{\rm ex}(L)$ in the form of sudden increase in the exchange bias field in the thickness region exceeding some critical value of L_c (Figure 1, a, b). Fast growth of the coercive force is also observed in the L_c region. This is a typical situation for exchange bias media [13]. It reflects the fact of growth with the antiferromagnetic crystallite thickness and at the same time indicates a variance of their sizes. According to our data obtained using an electron microscope on test samples without an FM layer, a columnar microstructure is typical to the Cr-Mn films. Bases of the columnar formations are parallel to the substrate plane and have a mean diameter of 35-40 nm that almost doesn't depend on the layer thickness (at least up to $L \sim 100\,\mathrm{nm}$). Thus, an increase in the antiferromagnetic layer thicknesses leads to a growth of the crystallite volume that is almost proportional to L. Turning back to the description of $H_{ex}(L)$ and $H_c(L)$, it can be assumed that when $L > L_c$ a considerable part of antiferromagnetic crystallites achieves a volume that provides their stability in ferromagnetic layer remagnetization conditions (see Equation (1)). They form the exchange bias. Smaller crystallites have no such stability and are switched together with the ferromagnetic layer, but hinder its remagnetization process and increase the coercive force accordingly. This particularly accounts for a large difference observed in the coercive forces of free films of the studied compositions H_c^* and similar layers in film composites H_c (see the table).

It follows from the curves shown in Figure 1 that L_c for films containing Fe layers is twice as high as for films with permalloy layers. This fact may be treated as reflection of stronger exchange interaction at the Cr-Mn/Fe interface

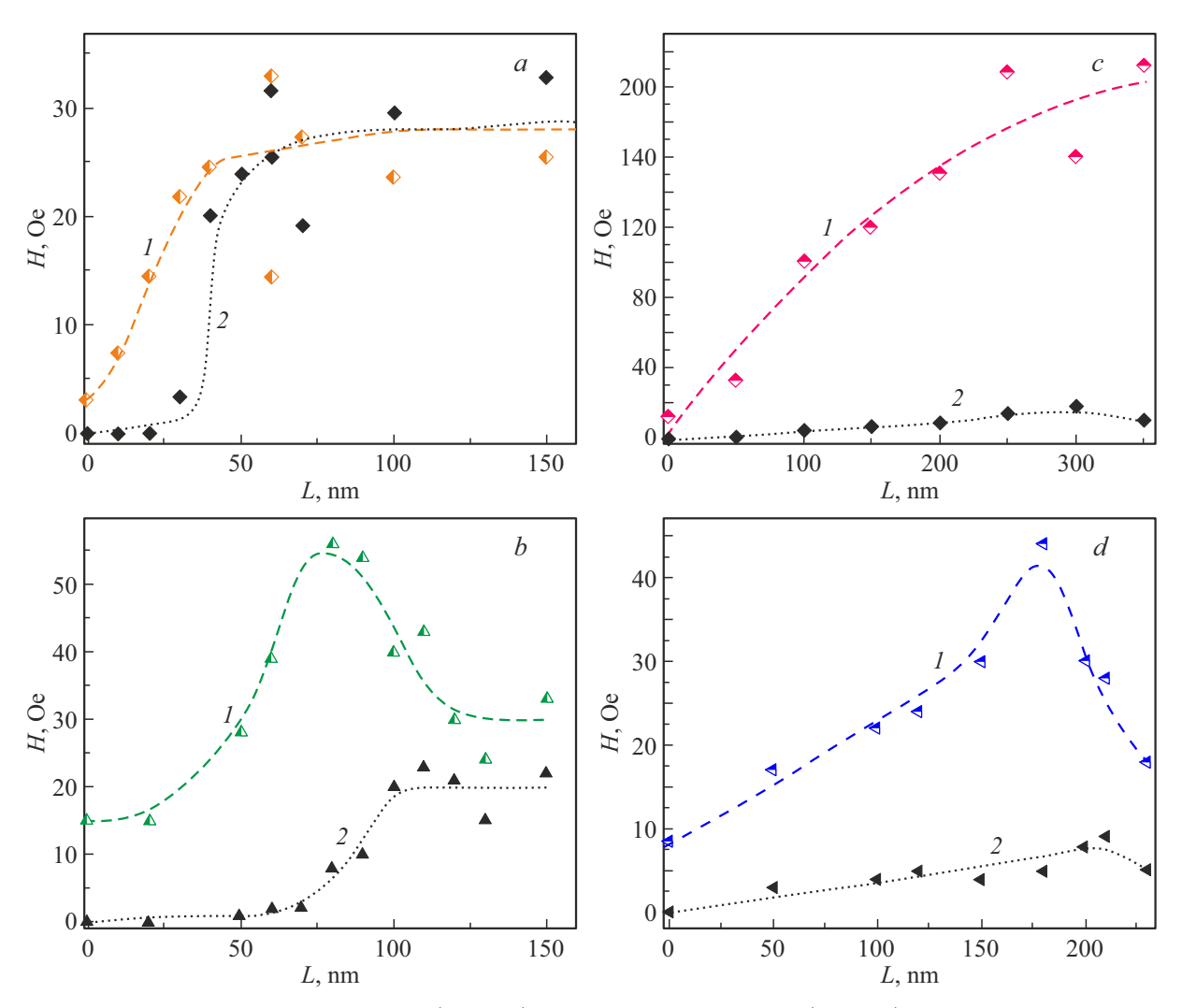


Figure 1. Dependences of the coercive force H_c (curves 1) and exchange bias field $H_{\rm ex}$ (curves 2) on the thickness L of the Cr–Mn layer for films with various ferromagnetic layers: Fe₂₀Ni₈₀ (a), Fe (b), Fe₁₀Co₉₀ (c), Fe₆₀Co₂₀B₂₀ (d).

than at the Cr-Mn/Fe $_{20}$ Ni $_{80}$ interface. It involves much larger antiferromagnetic crystallites in the process than in the permalloy layer case. Magnetic state stabilization of antiferromagnetic crystallites occurs at a relatively large volume and therefore $H_{\rm ex}(L)$ shifts towards larger thicknesses. Alongside with this, interaction with larger, but not yet stable crystallites causes a comparatively high coercive force of the Fe layers in the L_c region.

Interlayer coupling efficiency may be evaluated by the magnitude of H_{ex} using a known relation [23]

$$K_e = M_s \cdot H_{\rm ex} \cdot l, \tag{2}$$

where K_e is the coupling constant, M_s and l are spontaneous magnetization and ferromagnetic layer thickness, respectively. Results of this evaluation obtained using the tabulated spontaneous magnetization values of the corresponding alloys and l=10 nm are given in the table. As shown in the table, they confirm the above-mentioned statement about higher exchange coupling efficiency of the antiferromagnetic

Cr-Mn layer exactly with the Fe layer. "Harder" magnetism of Fe compared with permalloy probably displays itself in this. It is also not unlikely that crystalline affinity of the ferromagnetic and antiferromagnetic layers play a certain role. In the Cr-Mn/Fe case, both layers feature a BCC lattice with close parameters.

The second group includes films with ferromagnetic $Fe_{10}Co_{90}$ and $Fe_{60}Co_{20}B_{20}$ layers characterized by a smoother variation of the exchange bias field in a wide range of L and by a lower maximum level $H_{\rm ex}$. In the above logic, exchange coupling at the $Cr-Mn/Fe_{10}Co_{90}$ interface is presumably even stronger than in the cases mentioned above. It involves antiferromagnetic crystallites with even larger volume into the group of switchable crystallites. Therefore, the main effect of interlayer interaction translates into the coercive force growth, and the exchange bias field turns out to be small because it is formed by relatively few largest crystallites.

The given qualitative interpretation of results may be rephrased if the interlayer contact area is represented as a sum of two summands $S = s_c + s_e$, the former is provided by relatively small crystallites and is responsible for hysteresis and the latter, formed by larger crystallites, is responsible for exchange bias. Relation between s_c and s_e depends on the stability of antiferromagnetic crystallites and the efficiency of interlayer exchange interaction. An increase in the anisotropy constant and volume of antiferromagnetic crystallites leads to the growth of s_e and an increase in the interlayer exchange leads to the growth of s_c . Balance between these quantities affects the relation between H_c and $H_{\rm ex}$, but doesn't define their level completely. It also depends to a great extent on the energy expenditures of an external magnetic field for formation of the interlayer magnetic interface. The described conditions may be summarized by expanding the content of the coupling constant as $K_e = \lambda s_e / S$, where λ is the interlayer exchange parameter. Then, variation of ferromagnetic layer composition is functionally represented as variation of both λ and s_e . It follows that K_e is a generalizing quantity and its relatively low value for the Fe₁₀Co₉₀ layer (see the table) is consistent with the statement that the strongest interlayer exchange is implemented with its participation. Note also that the Fe₁₀Co₉₀ ferromagnetic material has a lattice, which is close to that of permalloy and, consequently, different from the Cr-Mn lattice. Therefore, the positive role of the affinity of antiferromagnetic and ferromagnetic layer lattices that was mentioned above may consist in the increase in s_e , and the interlayer exchange interaction itself described by λ primarily depends on the elementary composition of mating layers.

A composite material with amorphous ferromagnetic Fe₆₀Co₂₀B₂₀, another representative of the second group, demonstrates $H_{ex}(L)$ that is similar to that of Cr-Mn/Fe₁₀Co₉₀, but the maximum values of exchange bias and coercive force for it are lower (see Figure 1, c and the table). These facts cannot be interpreted un-On the one hand, a decrease in the ambiguously. hysteresis property level may be associated with the fact that addition of a considerable portion of boron to the Fe-Co ferromagnetic composition weakens the interlayer exchange interaction (reduces λ). But a monotonic increase in $H_{\rm ex}$ in the same wide range of L is somewhat inconsistent with this as in the Fe₁₀Co₉₀ case. On the other hand, amorphous nature of the structure is probably unfavorable for the effective magnetic contact between the ferromagnetic and antiferromagnetic layers. This may cause a decrease in the total number of antiferromagnetic crystallites involved in formation of hysteresis properties of the ferromagnetic layer, i.e. decrease in both s_c and s_e also takes place.

Threshold dependences $H_{\rm ex}(L)$ observed for $FM={\rm Fe_{20}Ni_{80}}$, Fe may be also used to evaluate the anisotropy constant of the antiferromagnetic layer based on

$$K_a \cdot V_e = K_e \cdot s_e, \tag{3}$$

where $V_e = L_c \cdot s_e$. Values of K_a calculated using (3) for structures with the Fe and Fe₂₀Ni₈₀ ferromagnetic layers turned out to be close to each other and were

equal to approximately $6 \cdot 10^4$ erg/cm³. Note that the obtained quantity is close to that found in [15] using a so-called York protocol [24] — $4 \cdot 10^4$ erg/cm³. Thus, it can be quite reasonably said that Cr–Mn is a low-anisotropy antiferromagnetic material and is considerably inferior in terms of this property to Ir–Mn, for which $K_a \sim 5 \cdot 10^6$ erg/cm³ [25] and which has found practical use in spin valves.

Figure 2 shows the dependences of hysteresis properties on the temperature T of film structures with various ferromagnetic layers obtained from the magnetometric hysteresis loops. The selected samples varied in the antiferromagnetic layer thickness that in each case corresponded to the highest value of H_{ex} that was preliminary determined at room temperature. The given data demonstrates the general trend for films with all FM layers that involves a decrease in the exchange bias field as T increases (Figure 2, curves 2). It primarily reflects the variation of relation between the magnetic anisotropy energy of antiferromagnetic crystallites and thermal fluctuation energy of their antiferromagnetic vector. Values of the blocking temperature T_b , at which the hysteresis loop shift disappears, though fall into a relatively small range of 500-600 K (see the table), but still vary considerably. Moreover, a certain pattern can be seen in this difference: the sample with the permalloy layer has the lowest T_b , the sample with the Fe layer has a medium Tb and the films with Co-containing layers have the highest Tb. Thicknesses of antiferromagnetic layers in these samples, with which the mean size of antiferromagnetic crystallites is associated, correlate in the same way. Hence, a natural conclusion can be made that crystallites with larger sizes provide high stability of their magnetic state with respect to thermal fluctuations and, consequently, high T_b .

Temperature dependences of the coercive force in films with different ferromagnetic layers look more specifically (Figure 2, curves 1) demonstrating a decrease $(FM = Fe_{20}Ni_{80})$ and non-monotonic variation $(FM = Fe_{10}Co_{90}, Fe_{60}Co_{20}B_{20})$ and growth of H_c as TTwo extreme cases may be interpreted as follows. When large crystallites are involved in the interlayer interaction and the exchange coupling is quite strong (λ) as is the case for $FM = \text{Fe}_{10}\text{Co}_{90}$, a part of them moves from the category of crystallites providing the exchange bias to the category of crystallites affecting the coercive force, i.e. redistribution of $s_e \rightarrow s_c$ occurs. Eventually, within the set test conditions $(T < 650 \,\mathrm{K})$, abnormally high coercive force level and ascending $H_c(T)$ are implemented. If the antiferromagnetic crystallites are small and the interlayer exchange is relatively weak ($FM = \text{Fe}_{20}\text{Ni}_{80}$), then $s_e \rightarrow s_c$ occurs with simultaneous effective decrease in s_c , and $H_c(T)$ is descending. For samples with two other FM layers, an intermediate situation probably occurs that is defined by the relation between the anisotropy energy of antiferromagnetic crystallites and the interlayer exchange. Temperature variation of their balance may be the cause of non-monotonic $H_c(T)$. An increase in the mean crystallite size with excessive heating and high-temperature interlayer

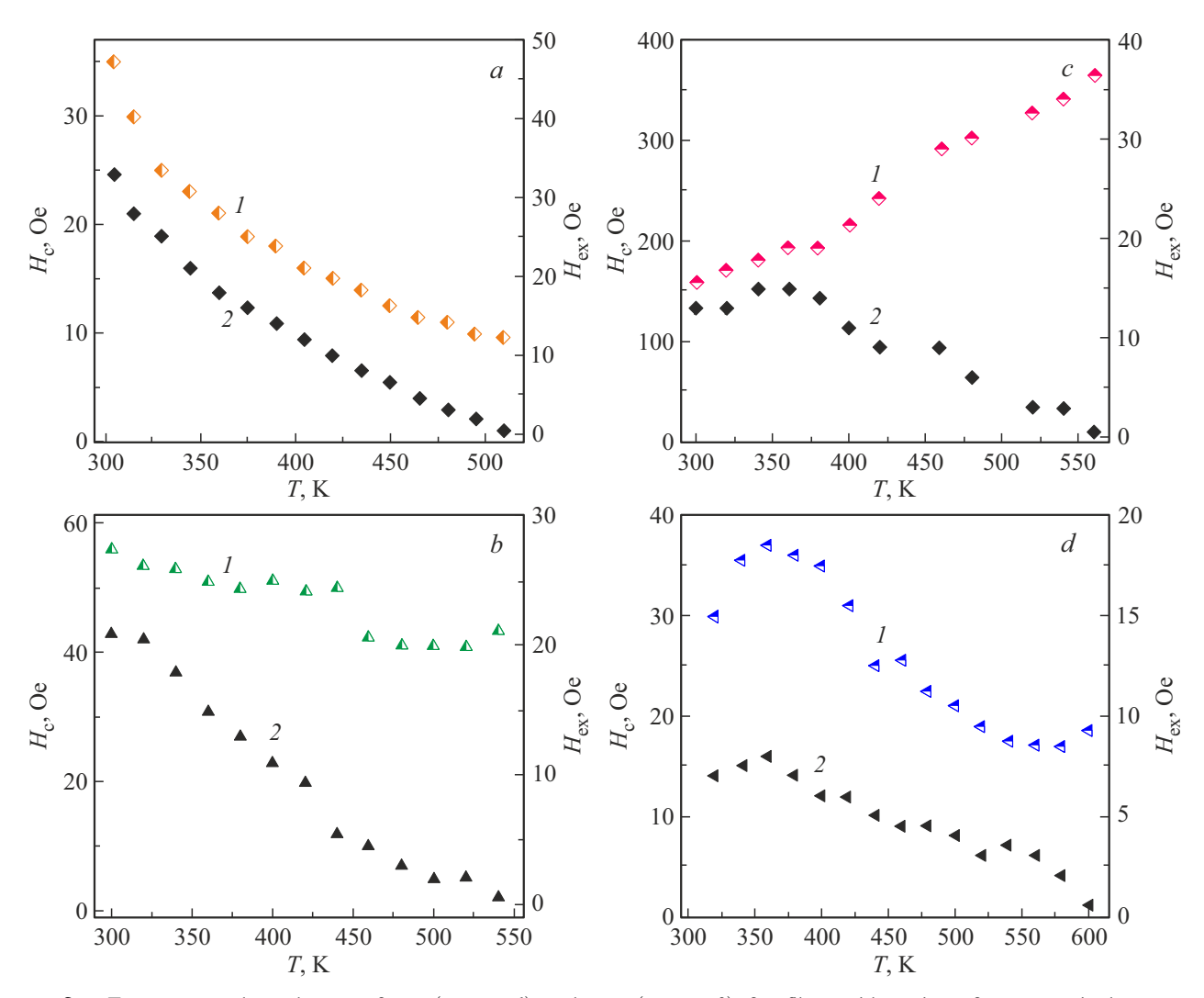


Figure 2. Temperature dependences of H_c (curves I) and $H_{\rm ex}$ (curves 2) for films with various ferromagnetic layers: $a - {\rm Fe}_{20}{\rm Ni}_{80}$ ($L = 50\,{\rm nm}$); $b - {\rm Fe}$ ($L = 100\,{\rm nm}$); $c - {\rm Fe}_{10}{\rm Co}_{90}$ ($L = 300\,{\rm nm}$); $d - {\rm Fe}_{60}{\rm Co}_{20}{\rm B}_{20}$ ($L = 210\,{\rm nm}$).

diffusion cannot be ruled out and may be displayed differently depending on a particular combination of layers [26].

As it follows from the data shown above the antiferromagnetic layer thickness plays an important role in formation of the exchange bias effect. The foregoing analysis is based on the fact that this coupling is induced by the thickness dependence of microstructure parameters, in particular, crystallite size and texture. To justify this provision, X-ray diffraction analysis and sample examination of the glass/ $Ta/Cr_{70}Mn_{30}(L)/Ta$ type films using an electron microscope were carried out. These samples didn't contain ferromagnetic layers due to an attempt to simplify the diffractometry data interpretation. Based on the existing experience, it can be also stated that Ta layers don't make any considerable contribution to the diffraction pattern of such films due small thickness and presumably amorphous state of Ta layers.

Figure 3, a shows diffraction patterns of films with different L. They show that a crystal structure close to the α -Cr structure is implemented in all studied samples.

The absence of a full set of corresponding diffraction lines indicates the crystal texture. Measurement of "rocking curves" or so-called ω -scans (see Figure 3, b) that allow reliable determining of texture has generally confirmed the presence of the (200) type texture in the thickness range of $20 < L \leq 250\,\mathrm{nm}$. At the same time, no any pronounced texture was found in the $L=300\,\mathrm{nm}$ sample, which was probably associated with irregularity of the columnar microstructure in thick films. The fact of particular texture of the Cr–Mn films is notable by itself, but, as reported earlier in our works [12,14], has no any paramount importance for formation of the exchange bias.

It's not the case with the crystallite volume, on which magnetic stability of crystallites depends as mentioned above. Results of the corresponding evaluation of the mean crystallite size D in the Cr—Mn films performed using the Scherrer equation [27] are shown in Figure 3, c. The absolute quantity D itself is quite provisional because it is defined by broadening of diffraction lines that are a generalized characteristic of the structural imperfection

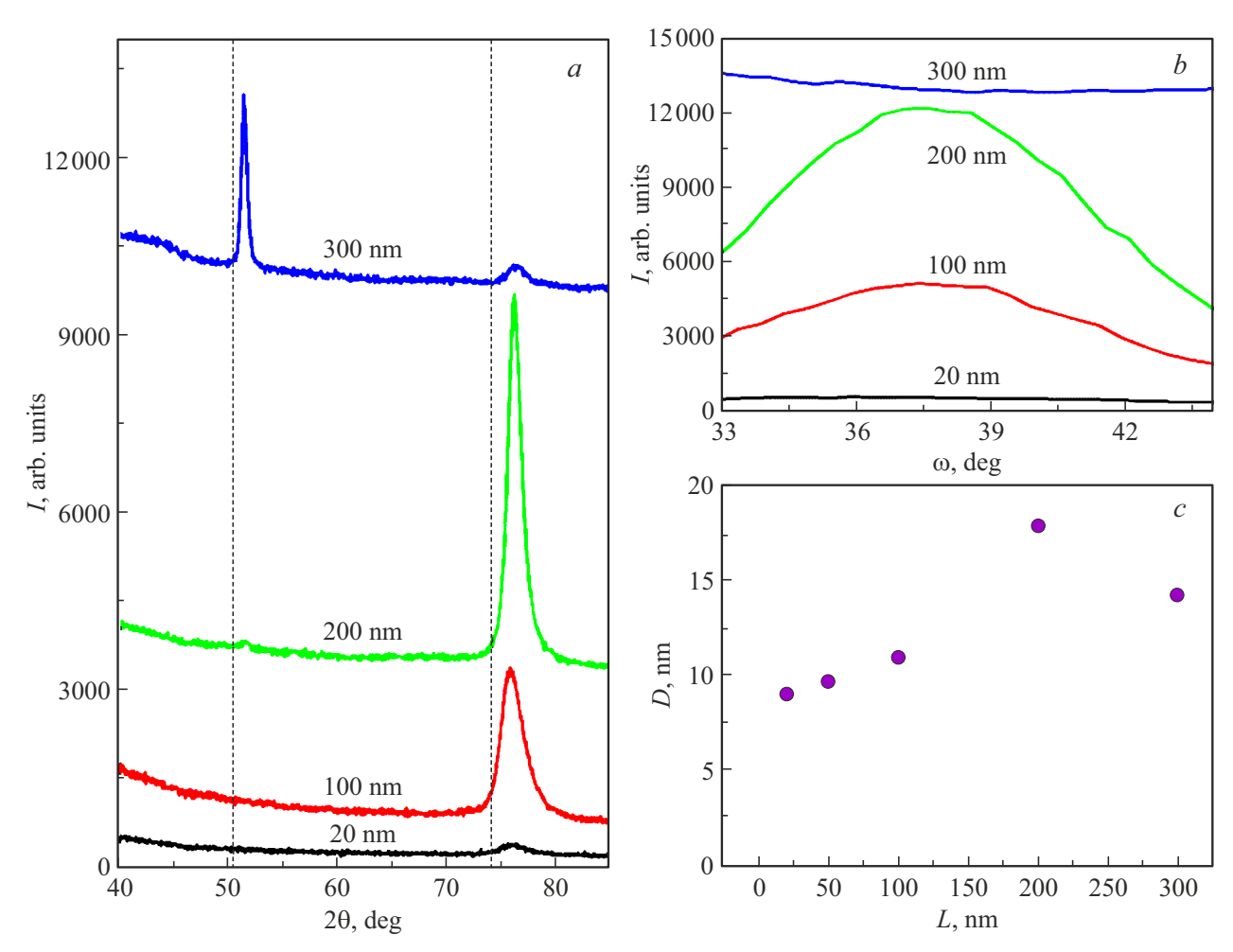


Figure 3. a — Diffraction patterns of the Ta/Cr₇₀Mn₃₀(L)/Ta with different L of the Cr–Mn layer. b — rocking curves of diffraction lines near the diffraction angle $2\theta = 75.50^{\circ}$. c — Dependence of the mean diameter of crystallites determined using the Scherrer equation on the Cr-Mn layer thickness.

of polycrystalline objects. A variation trend of D may be deemed to be a more adequate characteristic because it unambiguously indicates the increase in the size of crystallites with thickness and thus justifies the use of this factor for interpreting hysteresis properties of the studied film structures.

More details on the microstructure of the Cr-Mn films were obtained using the transmission electron microscopy (TEM) on samples deposited on soluble (NaCl) substrates. According to the TEM data, the Ta/Cr₇₀Mn₃₀/Ta films have a continuous island tiling morphology (Figure 4). Boundaries of faceted islands (shown by white circles) are well distinguished on the provided photos, and the variable contrast in cross-section may indicate their texture. Size of these formations coincides with the crystallite size and almost doesn't depend on the thickness of the Cr-Mn layers and the presence of a ferromagnetic layer (compare with Figure 4, a and 4, c), which indirectly confirms the columnar nature of the microstructure. The mean crystallite size evaluated from the provided photos is about 40 nm. Analysis of the corresponding electron diffraction patterns validates the X-ray diffractometry data regarding the prevalence of a phase in the films that is identified as α -Cr and allows the Cr₇₀Mn₃₀ binary composition to be identified as a solid solution. At the same time, the electron diffraction patterns have additional reflections indicating that there is some amount of MnO and MnO₂ in the samples. Judging by relative intensity of the lines, their content is low. It is not unlikely that they have occurred during the TEM examination because they are not identified in the X-ray diffraction patterns.

System film properties $(Cr_{70}Mn_{30})_{100-x}W_x/Fe_{20}Ni_{80}$

As mentioned above (see Equation (1)), the magnetic stability of antiferromagnetic crystallites together with the volume depends on the anisotropy constant of a substance, which can be controlled through doping. Figure 5, a shows the dependences of hysteresis properties of a permalloy layer included in film composite materials

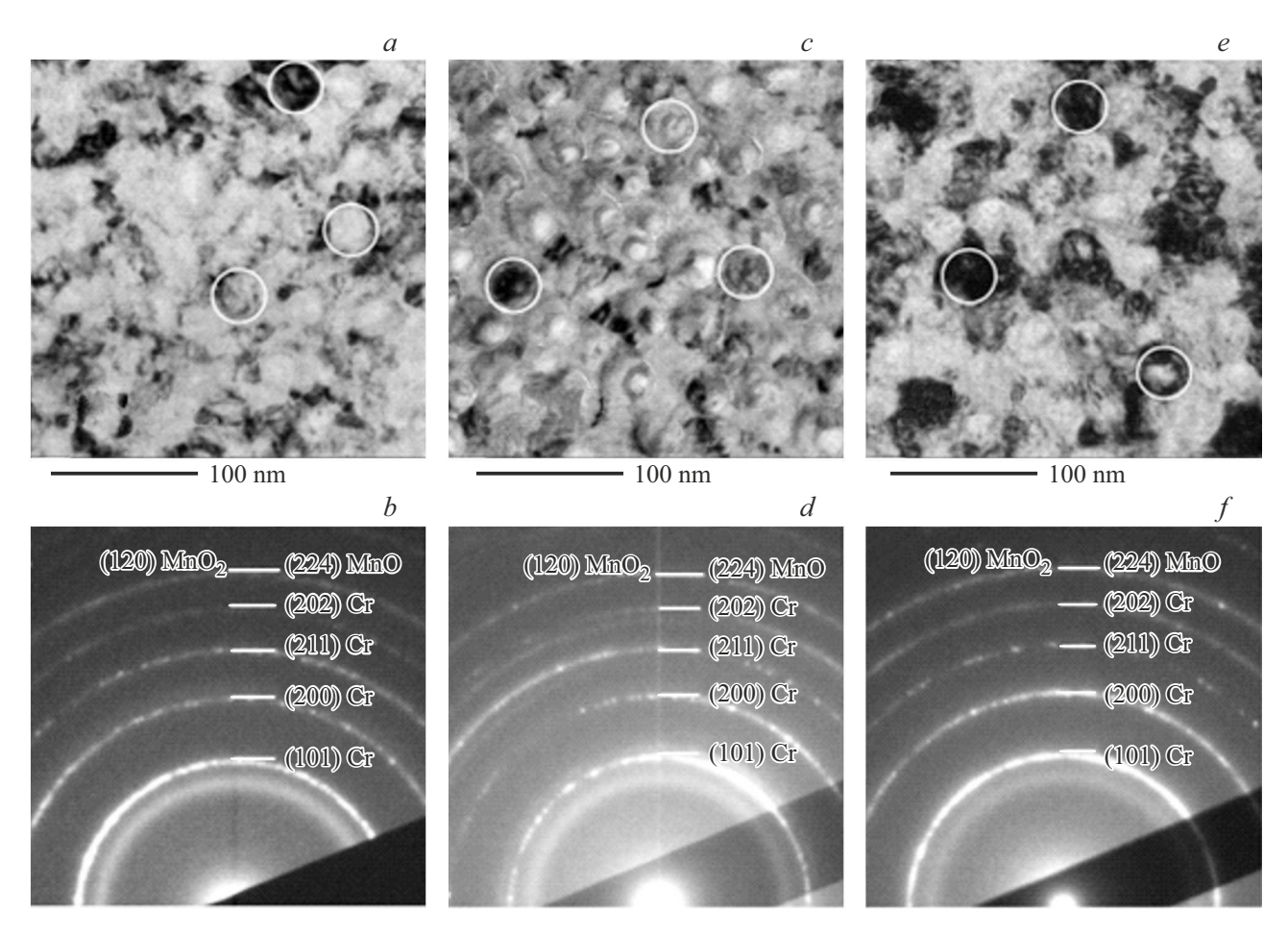


Figure 4. TEM photographs (a, c, e) and electron diffraction patterns (b, d, f) of the Ta/Cr₇₀Mn₃₀(L)/Ta films with L = 20 nm (a, b) and L = 50 nm (e, f), and of the Ta/Cr₇₀Mn₃₀(20)/Fe₂₀Ni₈₀/Ta film (c, d). White circles show typical structural elements that are individual crystals.

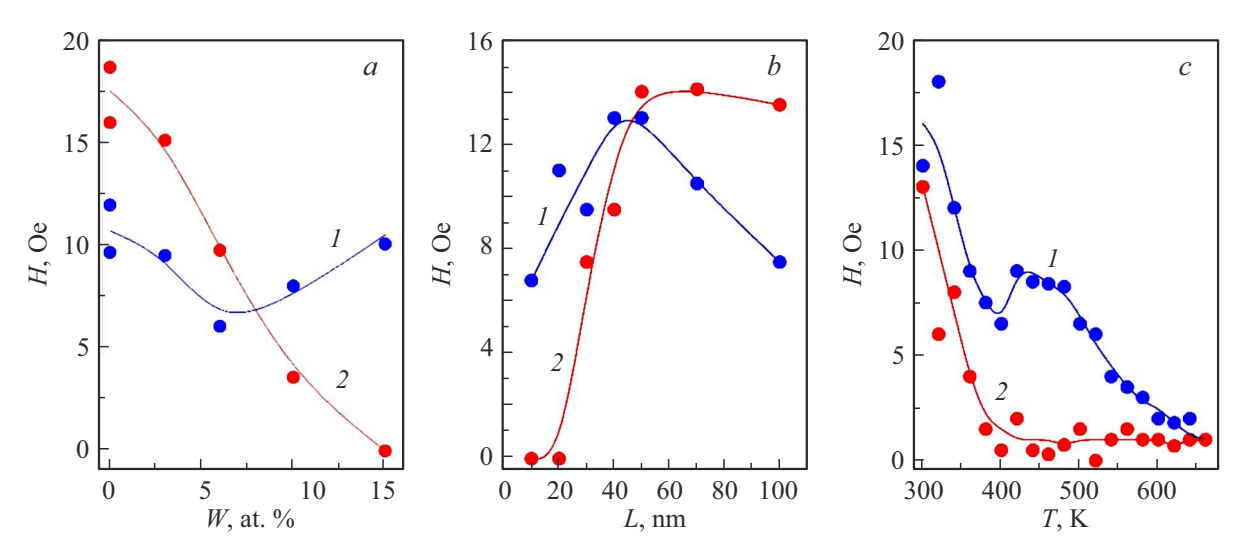


Figure 5. Dependences of the coercive force (curve I) and exchange bias field (curve 2) on the W concentration in $(Cr_{70}Mn_{30})_{100-x}W_x(50\,\text{nm})/Fe_{20}Ni_{80}$ films (a), on the antiferromagnetic layer thickness in $(Cr_{70}Mn_{30})_{95}W_5(L)/Fe_{20}Ni_{80}$ films (b) obtained at 300 K, and on the temperature in $(Cr_{70}Mn_{30})_{95}W_5(50\,\text{m})/Fe_{20}Ni_{80}$ films (c).

on the concentration of W that is used for doping the antiferromagnetic Cr₇₀Mn₃₀ layer. It is shown that the presence of a dopant doesn't enhance the pinning capability of antiferromagnetic crystallites. On the contrary, there is rather abrupt and almost linear decrease in the exchange bias field as the concentration of W increases. on the hysteresis property formation model of the studied composite materials that is described in the previous section, it can be concluded that such behavior of H_{ex} may be caused by a decrease in the mean crystallite size, magnetic anisotropy constant of the antiferromagnetic material or weakening of the interlayer interaction. Target experiments allowed a more definite judgement to be made regarding the role of W.

Figure shows the TEM photographs $Ta/(Cr_{70}Mn_{30})_{95}W_5$ (L)/Ta films with two thicknesses and the corresponding electron diffraction patterns. Comparison with similar data for undoped films (see Figure 4) shows that introduction of W induced particular structural changes. They were expressed in the appearance of considerable structural correlation between the columnar microstructure elements. This is evidenced by so-called zone-axial patterns in the form of intersecting dark lines observed on the TEM images and identified as bend extinction contours [28]. Corresponding dark field images show that doped films are a set of pseudo single-crystal regions whose lateral size within the specified contours is by an order of magnitude as high as the typical lateral dimension of the original columnar crystallites. Fragmentation of diffraction rings observed for doped films also indicates considerable growth of coherent scattering regions. Note also that the thickness of samples almost doesn't affect either the nature or quantitative parameters of the identified microstructure elements (compare Figures 6, a and 6, c) at least up to $L \sim 100$ nm.

The identified structuring features of the Cr-Mn-W films may be of individual interest, but are beyond the scope of this work. At the same time they are presumably of no direct significance for understanding the exchange bias formation mechanism. But note the substructure of pseudo single crystals. It is close to that observed in undoped films that have no zone-axial morphology (compare the photos in Figure 4 and Figure 6). Hence, it may be concluded that microstructural columnarity, that is probably also displayed through the corresponding surface texture, is maintained during doping and has close dimensional characteristics. It appears that the magnetic stability of exactly these formations affects the magnitude of exchange bias field. Otherwise, drastic coarsening of active structural elements of an antiferromagnetic material should have led to a corresponding increase in H_{ex} . Anyway, the absence of a decrease in the crystallite size excludes this factor from those that explain the decrease in H_{ex} during doping that is observed experimentally.

Magnetic anisotropy is another factor to be reviewed. Quantitative description of the magnetic anisotropy for antiferromagnetic materials is a difficult problem. Without solving the problem directly, a particular conclusion regarding the anisotropy constant variations during doping can be made through comparison of the thickness dependences of hysteresis properties of composite materials having the same ferromagnetic layers. Figure 5, b shows $H_{\rm ex}(L)$ and $H_c(L)$ for Ta/ $(Cr_{70}Mn_{30})_{95}W_5(L)/Fe_{20}Ni_{80}(_{10})/Ta$ films. It is shown that the exchange bias field variation has a near-threshold nature close and the coercive force in the region of drastic change of $H_{\rm ex}$ passes through the maximum. As noted above, such dependences are typical for ferromagnetic/antiferromagnetic composite materials and are similar to those shown in Figure 1, a for $Ta/(Cr_{70}Mn_{30}(L)/Fe_{20}Ni_{80}(10)/Ta$ films with undoped FM layers. There are apparent quantitative differences between them. On the one hand, 5% doping led to the shift of L_c to a lower value region (from 40 to 30 nm). Taking into account the absence of significant difference in the parameters of structural elements that provide the exchange bias in samples from different series and appealing to Equation (1), this result may be treated as a consequence of the increase in the magnetic anisotropy constant when W is added. However, on the other hand, the typical values and exchange bias and coercive force fields in samples containing the Cr-Mn-W layers are considerably lower, which is in some conflict with the statement regarding the increase in the magnetic anisotropy of an antiferromagnetic material. To resolve this conflict, it shall be assumed that doping can result in weakening of the interlayer exchange interaction (λ) and consequently of energy expenditures of a magnetic field for formation of magnetic interfaces (K_e) . Evaluations made using Equations (2) and (3) give 0.012 erg/cm² and $5 \cdot 10^{-4} \, \text{erg/cm}^3$ for K_e and K_a , respectively. Comparison with the same parameters of undoped films shows that the main effect from the introduction of W is in the decrease in the magnetic anisotropy constant, rather than in its increase, as believed initially. This probably also explains the downward trend in $H_{\rm ex}(x)$ and $H_{\rm c}(x)$ at the initial doping stage (see Figure 5, a). The rise undergone by H_c when x > 5% presumably reflects variations in the antiferromagnetic layer microstructure that have been discussed above. Note also that the discussed dependences in films with a doped antiferromagnetic layer differ in higher regularity and repeatability, which may result from the exchange bias effect shift towards lower antiferromagnetic crystallite sizes that are reproduced in a more stable manner within the employed technique.

Figure 5, c also shows the temperature dependences of hysteresis properties of the W-containing $(Cr_{70}Mn_{30})_{95}W_5(50)/Fe_{20}Ni_{80}$ film. Comparing them with the properties of a sample without W (see Figure 2), it may be stated that doping has led to a considerable decrease in T_b and some modification of $H_c(T)$. The latter has a clearly pronounced maximum in the T_b region that is typical of ferromagnetic/antiferromagnetic media, while the undoped sample has just a small kink in the same temperature Typically, the noted features are implemented against the background of a reduced hysteresis parameter

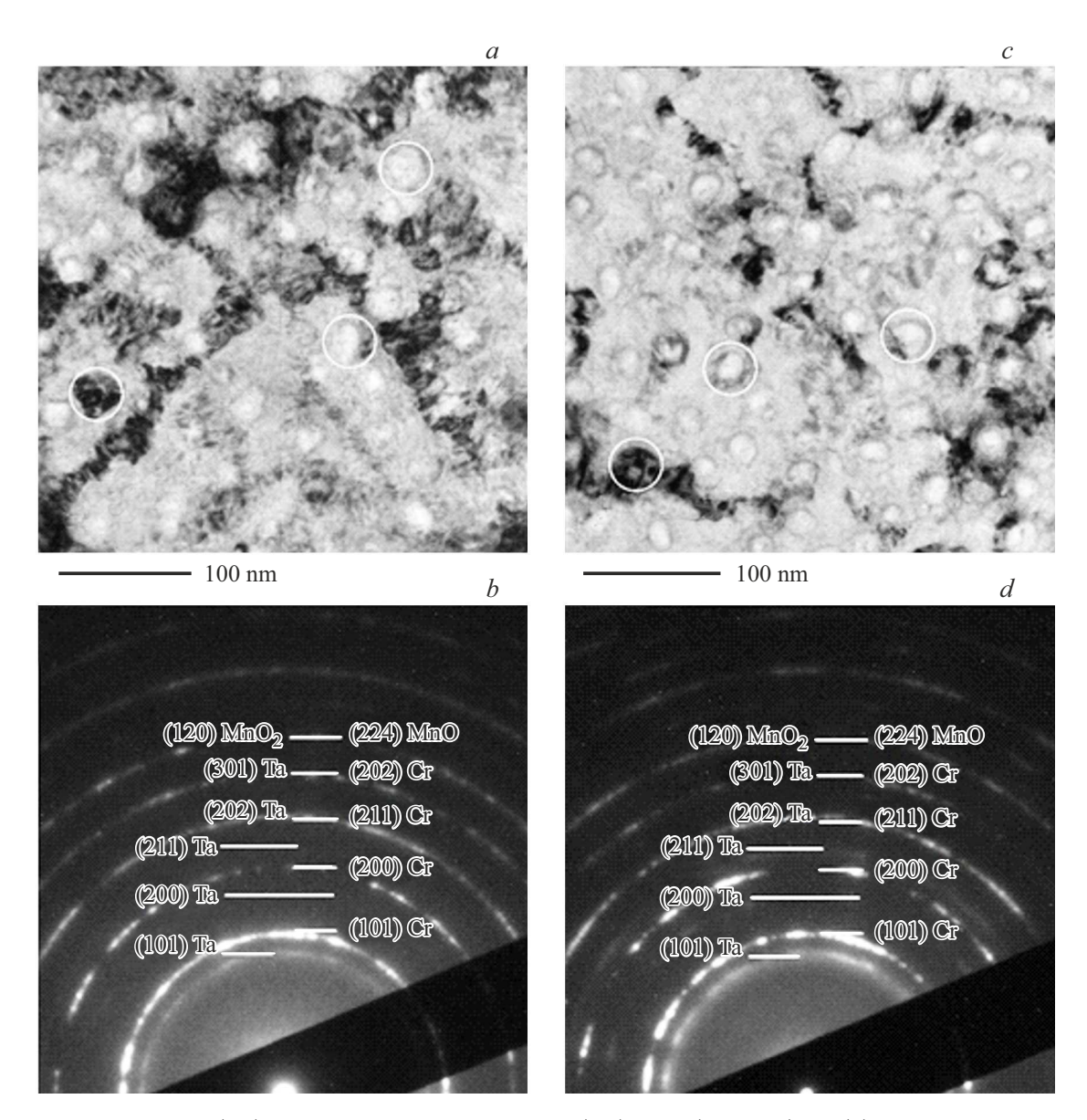


Figure 6. TEM photographs (a, c) and electron diffraction patterns (b, d) of $Ta/(Cr_{70}Mn_{30})_{95}W_5(L)/Ta$ films with L = 20 nm (a, b) and L = 50 nm (c, d). White circles show typical structural elements that are individual crystals.

level and are in agreement with the above conclusion regarding weakening of the magnetic anisotropy of the antiferromagnetic Cr–Ma films when W is introduced.

5. Conclusion

Results given in the work show that, along with a high Neel temperature, a stable magnetic state of crystallites with respect to the tilting action of the exchange-coupled ferromagnetic layer are important characteristics of an antiferromagnetic polycrystalline medium used for implementing the exchange bias effect. Combination study of the microstructure and hysteresis properties of the $Cr_{70}Mn_{30}/FM$ (FM = Fe, $Fe_{20}Ni_{80}$, $Fe_{10}Co_{90}$, $Fe_{60}Co_{20}B_{20}$) type films has shown that the stability of crystallites of the initially low-

anisotropy antiferromagnetic Cr-Mn may be controlled by varying the crystallite volume, magnetic anisotropy constant of the material or interlayer exchange efficiency. Such variation is performed by changing the antiferromagnetic layer thickness through W doping or selecting an FM layer material, respectively.

Funding

The study was funded by the Ministry of Higher Education and Science of the Russian Federation, project No. FEUZ-2024-0060.

Conflict of interest

The authors declare that they have no conflict of interest.

References

- D. Xiong, Y. Jiang, K. Shi, A. Du, Y. Yao, Z. Guo, W. Zhao. Fundam. Res. 2, 4, 522 (2022).
- [2] E.V. Gomonay, V.M. Loktev. Low Temp. Phys. **40**, *1*, 17 (2014).
- [3] R.L. Stamps. J. Phys. D: Appl. Phys. 33, 23, 247 (2000).
- [4] K. O'Grady, J. Sinclair, K. Elphick, R. Carpenter, G. Vallejo-Fernandez, M. I.J. Probert, A. Hirohata. J. Appl. Phys. 128, 4, 11 (2020).
- [5] S. Soeya, H. Hoshiya, R. Arai, M. Fuyama. J. Appl. Phys. 81, 9, 6488 (1997).
- [6] H. Chen, X. Ling, L. Ruiyu, L. Zicheng, L. Liu, H. Bingyang, L. Gongke, H. Yuling. Adv. Mater. 36, 14, 2310379 (2024).
- [7] B.H. Rimmler, B. Pal, S.J. Parkin. Nat. Rev. Mater. 10, 109 (2025).
- [8] A. Kohn, A. Kovács, R. Fan, G.J. McIntyre, R.C. Ward, J.P. Goff. Sci. Rep. 3, 1, 1 (2013).
- [9] A. Hirohata, T. Huminiuc, J. Sinclair, H. Wu, M. Samiepour, G.V. Fernandez, K. O'Grady, J. Balluf, M. Meinert, G. Reiss, E. Simon, S. Khmelevskyi, L. Szunyogh, R.Y. Díaz, U. Nowak, T. Tsuchiya, T. Sugiyama, T. Kubota, K. Takanashi, N. Inami, K. Ono. J. Phys. D: Appl. Phys. 50, 44, 443001 (2017).
- [10] R. Aidun, S. Arajs, C.A. Moyer. Physica Status Solidi **128**, *1*, 133 (1985).
- [11] Y. Hamaguchi, N. Kunitomi. J. Phys. Soc. Jpn. 19, 10, 1849 (1964).
- [12] V.O. Vaskovsky, A.A. Feshchenko, M.E. Moskalev, V.N. Lepalovsky, E.A. Kravtsov, A.N. Gorkovenko. ZhTF 93, 5, 679 (2023). (in Russian).
- [13] V.O. Vaskovsky, A.A. Bykova, A.N. Gorkovenko, M.E. Moskalev, V.N. Lepalovsky. ZhETF 165, 5, 665 (2024). (in Russian).
- [14] A.A. Feshchenko, M.E. Moskalev, A.N. Gorkovenko, V.N. Le-palovsky, E.A. Stepanova, E.A. Kravtsov, V.O. Vaskovsky. FTT 65, 6, 961 (2023). (in Russian).
- [15] A.A. Feshchenko, M.E. Moskalev, S.V. Severova, A.N. Gorkovenko, V.N. Lepalovsky, N.V. Selezneva, V.O. Vaskovsky. Fizika metallov i materialovedenie, 124, 9, 830 (2023). (in Russian).
- [16] M.E. Moskalev, A.A. Feshchenco, E.A. Kravtsov, E.V. Kudyukov, A.A. Yushkov, V.N. Lepalovskij, V.O. Vas'kovskiy. J. Magn. Magn. Mater. 596, 171958 (2024).
- [17] R. Yanes, O. Chubykalo-Fesenko, H. Kachkachi, D.A. Garanin, R. Evans, R.W. Chantrell. Phys. Rev. B. 76, 6, 064416 (2007).
- [18] K. Nishioka, S. Shigematsu, T. Imagawa, S. Narishhige. J. Appl. Phys. 83, 6, 3233 (1998).
- [19] H. Xia, R.M. White. J. Appl. Phys. 87, 1, 410 (2000).
- [20] S. Soeya, H. Hoshiya, K. Meguro, H. Fukui. Appl. Phys. Lett. **71**, *23*, 3424 (1997).
- [21] S. Soeya, H. Hoshiya, R. Arai, M. Fuyama. J. Appl. Phys. 81, 9, 6488 (1997).
- [22] A. Kashyap, P. Manchanda, P.K. Sahota, R. Skomski, J.E. Shield, D.J. Sellmyer. IEEE Trans. Magn. 47, 10, 3336 (2011).
- [23] A.A. Feshchenko, E.A. Stepanova, V.N. Lepalovskij, E.A. Kravtsov, V.O. Vas'kovskiy. AIP Publishing 2313, 1 (2020)
- [24] Z. Shi, J. Du, S. Zhou. Chin. Phys. B. 23, 2, 027503 (2013).

- [25] K. O'Grady, L.E. Fernandez-Outon, G. Vallejo-Fernandez. J. Magn. Magn. Mater. 322, 8, 883 (2010).
- [26] K.Y. Tsai, M.H. Tsai, J.W. Yeh. Acta Mater. 61, 1, 4887 (2013).
- [27] D.G. Cameron, A.L. Patterson UFN 22, 8, 442 (1939). (in Russian)
- [28] V.Y. Kolosov, A.R. Thölen. Acta Mater. 48, 8, 1829 (2000).

Translated by E.Ilinskaya